# Electrochemical behavior and electrolysis of Ru(III) in molten salts

Lei Wang, [ID] [ab] Hao Peng, [ID] [bc] Haiying Fu, [ID] [b] Yahui Wang, [ID] [a] Qiang Dou,*[b] Lifang Tian [ID] *[a] and Hailang Li[d]

The yield of [103]Ru in molten salt reactors is quite substantial and [103]Ru holds significant potential applications in nuclear medicine. The electrochemical method is a promising technique for extracting [103]Ru from molten salt reactor fuels. To investigate the electrolytic separation of [103]Ru in molten salts, this paper employed cyclic voltammetry (CV) and square wave voltammetry (SWV) to focus on the electrochemical behavior of Ru(III) at an inert tungsten electrode in LiCl–KCl. The results indicate that the reduction process of Ru ions in LiCl–KCl molten salt involves a two-step reaction: Ru(III) → Ru(II) → Ru(0). The diffusion coefficient of Ru ions was determined using cyclic voltammetry to be $1.65 \times 10^{-6}$ $cm^2$ $s^{-1}$. Constant-potential electrolysis was conducted at −2.5 V to obtain the electrolytic product, which was characterized by X-ray diffraction (XRD) and scanning electron microscopy with energy-dispersive spectroscopy (SEM-EDS). The deposited product was primarily composed of metallic ruthenium. According to inductively coupled plasma optical emission spectroscopy (ICP-OES) analysis, the extraction efficiency of Ru(III) ions on the nickel electrode reached 88.92%. The current efficiency was 58.93% for constant-potential electrolysis for 2 h. This study demonstrates that the separation of Ru by electrochemical methods in molten salts is feasible.

## 1 Introduction

One of the six IVth-generation reactor candidates, the molten salt reactor (MSR), is characterized by its use of molten salts serving dual functions as both nuclear fuel carriers and reactor coolants. This unique design eliminates the need for fabricated fuel elements while enabling real-time fuel replenishment and online processing. When integrated with dry separation, MSRs hold great promise for achieving closed nuclear fuel cycles.[1]

The operation of molten salt reactors generates an array of fission products whose half-lives, spatial distribution, and physicochemical behaviors are various.[2] According to their chemical behavior in the reactor, the fission products were roughly divided into three categories by the Oak Ridge National Laboratory (ORNL):[3] the noble gases (Kr and Xe), the salt-seekers (Cs, Sr, Zr, *etc.*) and the noble metal fission products (Nb, Mo, Ru, *etc.*), whose behavior is very complicated and unpredictable.[4,5] Notably, some fission products such as [99]Mo–[99m]Tc, ^{68}Ga, ^{177}Lu, and ^{131}I have been extensively utilized in clinical nuclear medicine for targeted organ imaging, diagnostic procedures and therapeutic applications.

The decay product [103m]Rh of [103]Ru can emit Auger electrons,[7] which have important applications in nuclear medicine.[6] Due to its high Auger electron yield, short half-life (56 min), and ultrashort tissue penetration range (nanoscale cytotoxicity),[7] [103m]Rh has the potential to become a landmark radionuclide for Auger electron therapy in the targeted treatment of various cancers such as prostate cancer, neuroendocrine tumors, and gliomas.[8] [103]Ru also has potential applications in nuclear medicine. It finds application in both diagnostic imaging of adrenal dysfunction[9] and therapeutic management of thyroid carcinoma,[11] while simultaneously exhibiting significant potential for diagnosis and treatment.[10] The availability of [103m]Rh is directly dependent on the production capacity of [103]Ru, which currently faces limited global supply. The current production of [103]Ru is based on irradiation techniques, including the use of nuclear reactors and particle accelerators. In the reactor, the fission yield of [103]Ru can reach 3.1%. As a liquid fuel reactor, [103]Ru has a considerable yield in molten salt reactors due to whole-reactor irradiation. The output of molten salt reactors has been proved to be dozens or even hundreds of times that of other production methods.[6] Consequently, separating [103]Ru from molten salt reactor fuel offers a highly potential option, making it an attractive source for this nuclide.

The physicochemical behavior of [103]Ru in molten salt reactors exhibits considerable complexity. ORNL studied the distribution of [103]Ru in molten salt reactors by measuring the

*aSchool of Chemistry and Molecular Engineering, Nanjing Tech University, Nanjing 211816, P. R. China. E-mail: tianlifang@njtech.edu.cn*

*bShanghai Institute of Applied Physics, Chinese Academy of Sciences, Shanghai 201800, P. R. China. E-mail: douqiang@sinap.ac.cn*

*cWuwei Institute of Advanced Energy, Wuwei 733000, Gansu Province, P. R. China*

*dDepartment of Pharmacy, Diamond Medical College, Xiamen 361023, P. R. China*

pump bowl using γ-ray spectroscopy.[5] Research findings indicate that [103]Ru exhibits multifaceted distribution in molten salt reactors. Portions of [103]Ru dissolve in the molten salts, while others precipitate in the off-gas stream and on the surfaces of structural materials. This demonstrates the highly complex distribution of [103]Ru in molten salt reactors. Through systematic γ-ray spectroscopic analysis of molten salt systems, Cheng et al.[12] proved that only a small amount of [103]Ru existed in the molten salt in a dissolved state, while most of them were enriched in the gas–liquid or solid–liquid interface region in the form of a metallic state.

Dry separation is suitable for separation of nuclide from MSR fuel salts and it mainly includes fluoride volatility separation, reductive extraction, and electrochemical separation techniques. ORNL successfully extracted uranium in the fuel salt of molten salt reactors using fluorination volatilization, resulting in uranium mass loss of less than 0.1 wt%.[13] This method is suitable for substances with low boiling points of fluorinated products, whereas ruthenium fluorides have high boiling points (∼230 °C). ORNL has also successfully separated protactinium and rare earth fission products[14] using reductive extraction. The French Atomic Energy Commission (CEA) effectively separated actinides and lanthanides using reductive extraction, with actinide recovery rate reaching 99%.[15] However, the processing flow for reduction extraction in engineering applications is relatively complex. Electrochemistry utilizes the potential difference between separated elements to achieve the separation of target elements.[16,17] This method is characterized by its rapid response, real-time capability, and suitability for high-temperature, highly radioactive molten salt environments.[18] Furthermore, the molten salt electrodeposition[35,36] method has now reached a relatively mature stage of development. It is suitable for the extraction and separation of various metals. Electrochemical methods have been successfully applied for the separation of high-concentration U,[19–24] Th[25–27] and low concentrations of rare earth elements[28–34] in molten salts. Consequently, molten salt electrochemistry showcases the prospects in ruthenium separation in molten salt reactor systems.

Ruthenium exhibits a relatively strong electronegativity,[37] which provides a strong justification for the electrolytic separation of ruthenium. Research has already been conducted on the extraction of ruthenium using electrochemical methods. As shown by Kobayashi et al.,[38] the electrodeposition of ruthenium from ruthenium chloride and ruthenium nitrosyl chloride solutions has been studied and this electrodeposition method has been employed to separate radioactive ruthenium from fission products. Pravati Swain et al.[39] investigated the electrochemical behavior of ruthenium on a platinum electrode in nitric acid solution and successfully extracted ruthenium by potentiostatic electrolysis. The electrodeposition behaviors of nitrosyl ruthenium in nitric acid solution were systematically investigated by Rui Zou et al.[40] using electrochemical quartz crystal microbalance analysis and cyclic voltammetry. The results show that the reduction of ruthenium is achieved in steps. From the above analysis, it can be seen that most electrochemical studies on ruthenium have been conducted in aqueous solutions. However, the aqueous solution method is not suitable for separating nuclides from molten salt reactor fuel salts, as they generate significant amounts of waste liquid.

However, relative studies on molten salt systems are rarely reported. Currently, existing research remains relatively preliminary. Current research primarily confirms, through electron absorption spectroscopy (EAS) and electrochemical methods,[41–43] that ruthenium predominantly exists stably in molten salts as octahedrally coordinated +3 ions. Osipenko's research[42] results indicate that the reduction process of ruthenium in chloride melts based on LiCl–KCl and LiCl–KCl–CsCl eutectics occurs in a single step. G. Kartal Sireli[44] further explored the process of electrodepositing ruthenium coatings in LiCl–KCl molten salts using a two-electrode system.

Moreover, current research has not systematically investigated electrochemical behavior and electrolytic processes and electrochemical parameters such as the diffusion coefficient and reversibility of ruthenium are also lacking. Furthermore, previous studies have demonstrated that the reduction process in LiCl–KCl molten salts occurs in a single step, which contradicts the traditional two-step reduction mechanism for transition metals.

Fluoride molten salts typically face limitations such as uncontrollable costs in raw material preparation and purification. In contrast, chloride molten salts offer advantages including lower melting points, wider sources, and better controllability of impurities. In particular, the broad electrochemical window of chloride systems provides crucial thermodynamic and kinetic foundations for the study of the electrochemical behavior and separation of ruthenium elements. In this paper, a LiCl–KCl system is selected primarily due to its lower melting point, reduced corrosivity, and similar thermophysical properties to fluoride salts (FLiBe). Thus, experimental results from LiCl–KCl can provide valuable references for fluoride salt systems.[47]

In this work, cyclic voltammetry (CV) and square wave voltammetry (SWV) were used to systematically investigate the electrochemical behavior of Ru in LiCl–KCl molten salts using a three-electrode system, obtaining key parameters including redox potentials, reversibility, and diffusion coefficients. During the electrolysis process, the three-electrode system maintains a more stable electrolytic potential compared with the two-electrode system, ensuring the smooth progression of the electrolysis process and eliminating the effects of ohmic drops in the electrolyte.[45,46] Based on the above data analysis, constant-potential electrolysis was executed to obtain electrolytic products at appropriate conditions. Finally, the composition of the electrolytic products was analyzed by a number of characterization tools, including X-ray diffraction (XRD) and scanning electron microscopy with energy-dispersive spectroscopy (SEM-EDS) for composition and morphology analysis. Furthermore, the electrolysis efficiency of the whole electrolysis process and the feasibility of electrolytic separation of Ru were evaluated, which provided a scientific basis for the subsequent development of an effective electrolytic separation process.

# 2  Experimental

## 2.1.  Chemicals

LiCl (≥99.5%), KCl (≥99.8%), RuCl$_3$ (99.6%), tungsten wire ($\varphi$ = 1 mm, 99.9%), silver wire ($\varphi$ = 1 mm, 99.9%), Ni sheet ($\Phi$ = 20 mm × 10 mm×1 mm, 99.9%), and absolute ethanol were provided by Sinopharm Chemical Reagents Co., Ltd. Tungsten (W) was selected as the working electrode because it is an inert electrode that does not form a Ru–W alloy with ruthenium at 773 K in Fig. 1.[48]

## 2.2.  Preparation and purification of molten salt materials

The highly purified LiCl–KCl (52 : 48 mol%) eutectic mixture (>99.9%) was synthesized by thoroughly mixing dried LiCl (44 g) and KCl (56 g), then placing the mixture in a graphite crucible ($\Phi$ = 50 mm × $H$ 40 mm) within a sealed furnace. The furnace was heated to 300 °C for 5 h to remove the absorbed water, followed by heating to 500 °C for 24 h to ensure complete melting. After cooling to room temperature, the prepared eutectic salt was characterized for impurities by ICP-OES. The main impurity analysis results for the LiCl–KCl molten salt are shown in Table 1. These results demonstrate that the prepared molten salt exhibits high purity and low impurity concentrations, making it suitable for electrochemical research. Ru(III) ions were introduced into the LiCl–KCl salt in the form of RuCl$_3$ powder. The mixture of RuCl$_3$ and LiCl–KCl (RuCl$_3$ : LiCl–KCl = 1 : 99 mol%) was homogenized in a graphite crucible and heated at 300 °C for 1 h to remove residual moisture, followed by heating at 500 °C for more than 6 h.

## 2.3.  Electrochemical analysis and setup

### 2.3.1.  Electrochemical device and three-electrode system.
All electrochemical measurements were conducted in a three-electrode system. The working electrode was a tungsten wire ($\varphi$ = 1 mm, 99.9%), polished with SiC sandpaper, ultrasonically cleaned with deionized water and ethanol, and dried. The

**Table 1**  Concentration of main impurities in LiCl–KCl molten salt

| Element | Concentration/ppm |
| --- | --- |
| Mg | 3 |
| Cu | 3 |
| Al | 4 |
| Fe | 1 |
| Ni | 5 |
| Cr | 1 |

counter electrode was a graphite rod ($\varphi$ = 5 mm, 99.9%). The carbon powder on the surface of the stone mill rod was wiped clean with soft paper, ultrasonically washed with deionized water and ethanol, and then dried and placed in a glove box. The Ag/AgCl reference electrode was prepared by inserting a spiral-wound silver wire into an alumina tube.[49] The sealed end was ground until porous using sandpaper or a grinding wheel. A mixture of LiCl–KCl–AgCl (1.0 mol%) salt was packed into the modified alumina tube. The assembled electrode was then immersed in molten electrolyte for 24 h until stable electrochemical signals were detected. All electrochemical experiments were conducted using an Autolab electrochemical workstation controlled by Nova 2.1 software. All experiments were conducted in an argon-filled glovebox (99.999% purity) with H$_2$O and O$_2$ levels maintained below 0.5 ppm to prevent oxidation and moisture absorption of ruthenium products. The experimental setup is illustrated in Fig. 2.

### 2.3.2.  Electrochemical measurements.
Cyclic voltammetry (CV) and square wave voltammetry (SWV) were utilized to study the electrochemical behavior of Ru(III) in LiCl–KCl molten salt
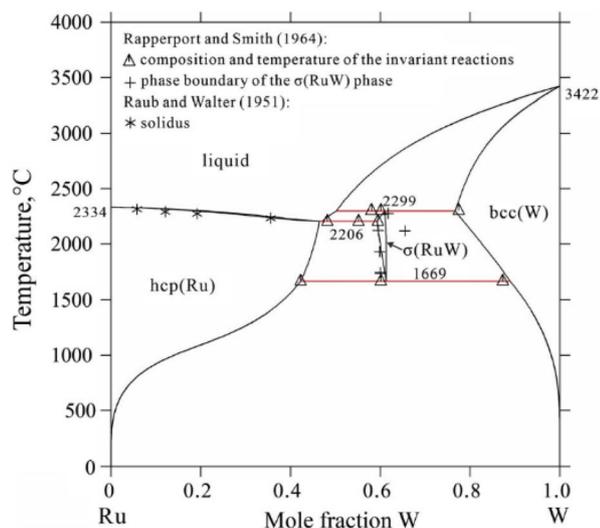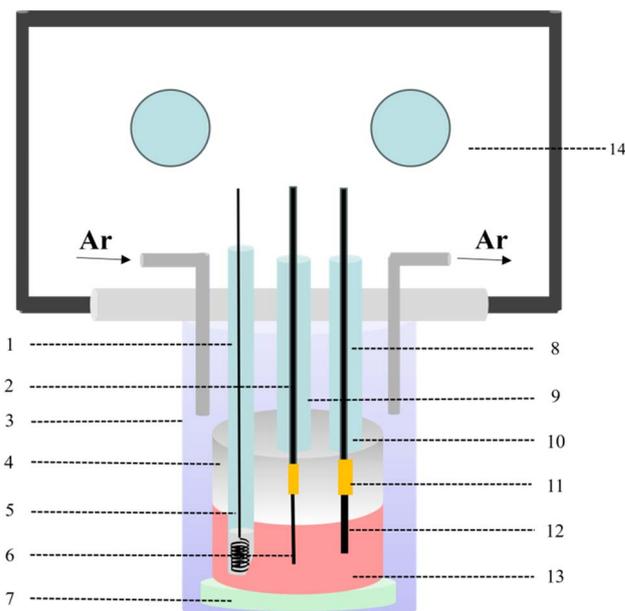


**Fig. 1**  Ru–W binary phase diagram.[48]



**Fig. 2**  Schematic diagram of electrochemical cell (1: reference electrode; 2: stainless steel wire; 3: electric furnace; 4: graphite crucible; 5: silver wire; 6: tungsten wire; 7: alumina gasket; 8: corundum tube; 9: working electrode; 10: counter electrode; 11: copper connector; 12: graphite rod; 13: molten chloride; 14: glove box).
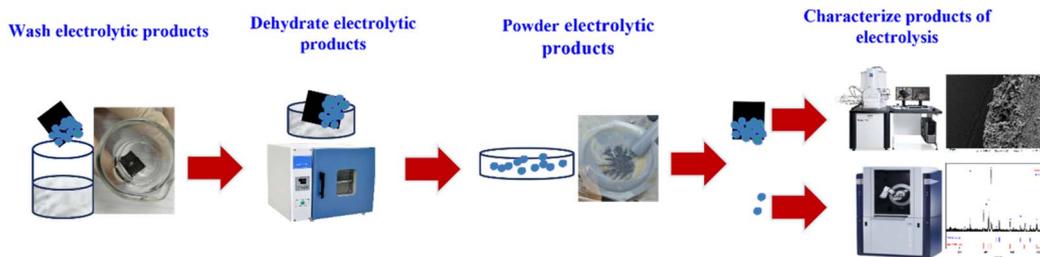
**Fig. 3** The treatment process for electrolytic products.

to obtain the key electrochemical parameters, such as redox peak potentials, peak currents, diffusion coefficients, electrode reaction mechanism, reversibility, *etc.*

**2.3.3. Electrolysis experiments.** Based on the electrochemical behavior studies, electrolytic separation experiments were further conducted using a three-electrode system. In this setup, a nickel plate functioned as the working electrode, graphite as the counter electrode, and a Ag/AgCl electrode as the reference electrode. The experiments were performed under a constant potential, with electrolysis lasting for 2 hours, to systematically examine the electrolytic separation behavior.

## 2.4. Characterization of electrolytic products

**2.4.1. Pre-treatment of electrolytic products.** Electrolytic products were obtained using constant-potential electrolysis. The products underwent ultrasonic cleaning to remove surface salts, followed by vacuum drying to dry the samples. Then the obtained electrolytic product samples were transferred for further analysis. The treatment process for electrolytic products is shown in Fig. 3.

**2.4.2. Chemical analysis.** The deposits were analyzed by X-ray diffraction (XRD; DY3616, X'Pert Powder), and the morphology and element distribution of the surface and cross-section of the deposits and the electrode after electrolysis were characterized by scanning electron microscopy with energy-dispersive spectroscopy (SEM-EDS; Merlin compact). The

sample preparation and pretreatment procedures for the above characterization techniques are detailed in ref. 50.

Additionally, inductively coupled plasma optical emission spectroscopy (ICP-OES; Optima 8000) was used to measure Ru(III) concentration in the molten salt before and after electrolysis. The sample preparation process prior to characterization is as follows. Samples of the melt were collected by immersing a quartz tube ($\Phi$6 mm) into the melt. After cooling, the sample was ground to a powder using a mortar. Subsequently, 0.1 g of the fine powder was weighed in a glove box and transferred into a graphite digestion block. Following the addition of 2% (v/v) $HNO_3$,[51] the vessel was placed in a graphite digestion system and heated to 90 °C for 4 hours until complete dissolution. After cooling to room temperature, the sample solution was transferred to a 50 mL centrifuge tube and further diluted with 2% $HNO_3$. The ruthenium content in the dissolved sample was then determined using inductively coupled plasma emission spectroscopy (ICP-OES).

# 3 Results and discussion

## 3.1. Electrochemical behavior of Ru(III) ions in molten LiCl–KCl

**3.1.1. Cyclic voltammetry.** Fig. 4(a) shows the cyclic voltammetry test curve of LiCl–KCl molten salt system at 773 K using a W electrode. Only the redox peak of $Li^+$ in the LiCl–KCl
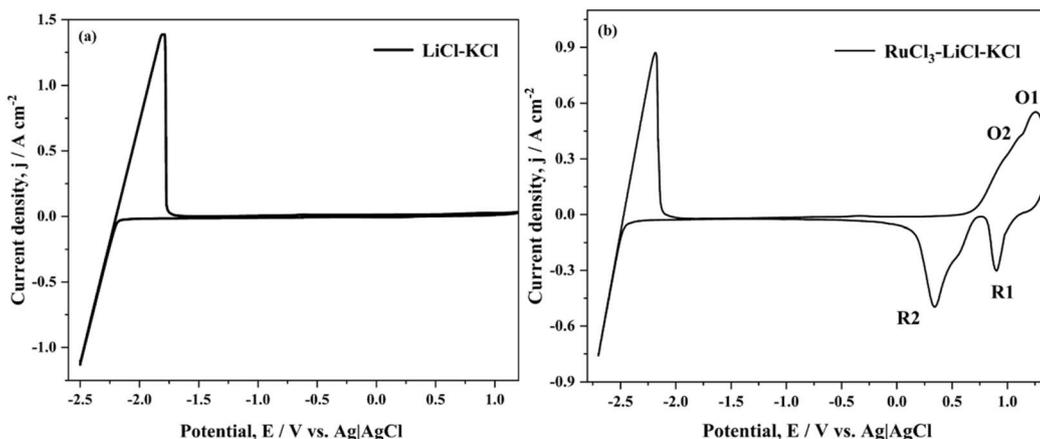


**Fig. 4** (a) Cyclic voltammetry curves of the LiCl–KCl and (b) LiCl–KCl–RuCl$_3$ ($1.13 \times 10^{-4}$ mol cm$^{-3}$) systems at 773 K with a scan rate of 0.1 V s$^{-1}$ (working electrode: W electrode, surface area: 0.32 cm$^2$; counter electrode: graphite rod ($\Phi$5.0 mm)).
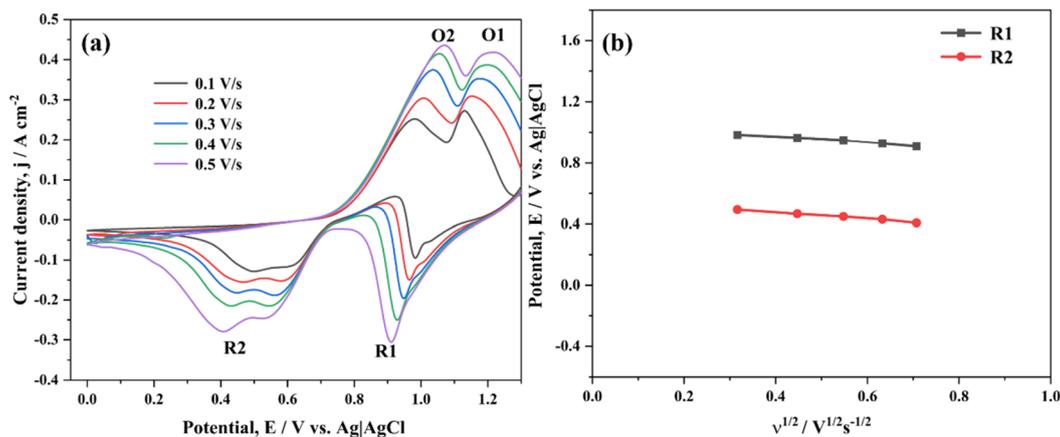
**Fig. 5** (a) Cyclic voltammetric curves of LiCl–KCl–RuCl$_3$ ($1.13 \times 10^{-4}$ mol cm$^{-3}$) molten salt at different scan rates. (b) Dependence of reduction peak potential on the square root of the scan rate for R1 and R2 for a W electrode in LiCl–KCl–RuCl$_3$ ($1.13 \times 10^{-4}$ mol cm$^{-3}$) eutectic at 773 K (working electrode: W electrode, surface area: 0.32 cm$^2$; counter electrode: graphite rod ($\Phi$5.0 mm)).

molten salt potential window, with no other extraneous peaks observed. This indicates that the LiCl–KCl used in the experiment is of high purity and is suitable for conducting molten salt electrochemical experimental analysis and testing. Fig. 4(b) records the CV curve of LiCl–KCl–RuCl$_3$ molten salt on the W electrode. It can be seen from the CV curve that in addition to the redox peak of Li$^+$, two pairs of sharp redox peaks, R1/O1 and R2/O2, are observed. The potentials for the reduction peaks appeared at 1.003 V for R1 and 0.660 V for R2, while the oxidation peaks O1 and O2 appeared at 1.067 V and 1.213 V, respectively. Only RuCl$_3$ was incorporated into this system; hence, these two pairs of redox peaks are attributed to the Ru(III) species at the electrode. These results suggest that the reaction process of Ru(III) at the electrode proceeds primarily in two steps.

To further study the characteristics of these peaks more, CVs were conducted at different scan rates within a narrow potential range, and the results are shown in Fig. 5(a) and (b). As the scan rate increased, the potentials of reduction peaks R1 and R2 shifted slightly towards the negative direction. There is a small

peak near the reduction peak R2 on this cyclic voltammetry curve, which should be attributed to the monolayer adsorption and desorption of Ru on the working electrode. The similar phenomenon was also observed in ref. 52 and 53. Furthermore, the current density of the reduction peaks R1 and R2 exhibited a linear relationship with the square root of the scan rate in Fig. 6(a) and (b). These observations demonstrate that R1 and R2 represent quasi-reversible processes throughout the entire procedure.

**3.1.2. Square wave voltammetry.** Compared to cyclic voltammetry, square wave voltammetry is a methodology that enables more sensitive and precise electrochemical analysis, enabling accurate determination of the number of transferred electrons involved when an electrochemical process occurs. In order to more accurately study the reduction mechanism of the two-step electrode reaction of Ru(III), a higher sensitivity and more accurate SWV was used for testing.

As illustrated in Fig. 7(a), SWV tests were conducted at 15 Hz and the test results were fitted using a Gaussian fitting. This confirms that two steps of reduction occurred during the
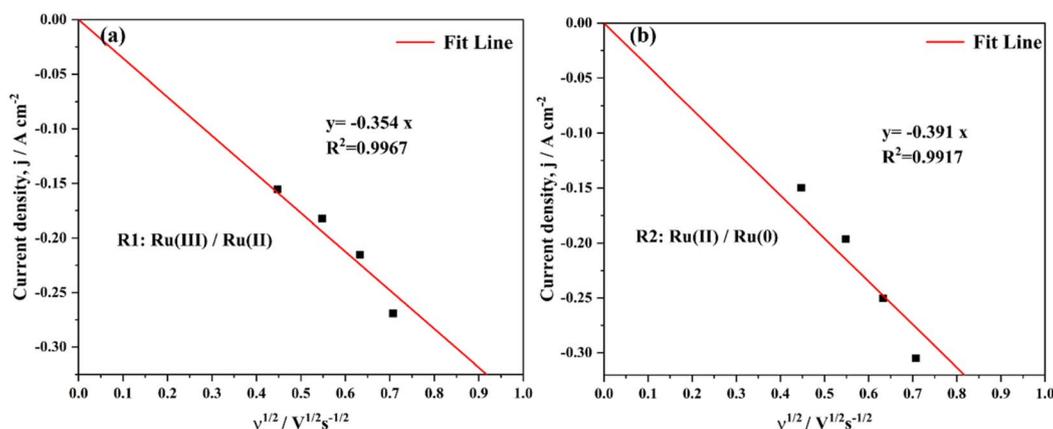


**Fig. 6** Dependence of current density of the reduction peak R1 (a) and R2 (b) on the square root of the scan rate in LiCl–KCl–RuCl$_3$ ($1.13 \times 10^{-4}$ mol cm$^{-3}$) eutectic at 773 K (working electrode: W electrode, surface area: 0.32 cm$^2$; counter electrode: graphite rod ($\Phi$5.0 mm)).
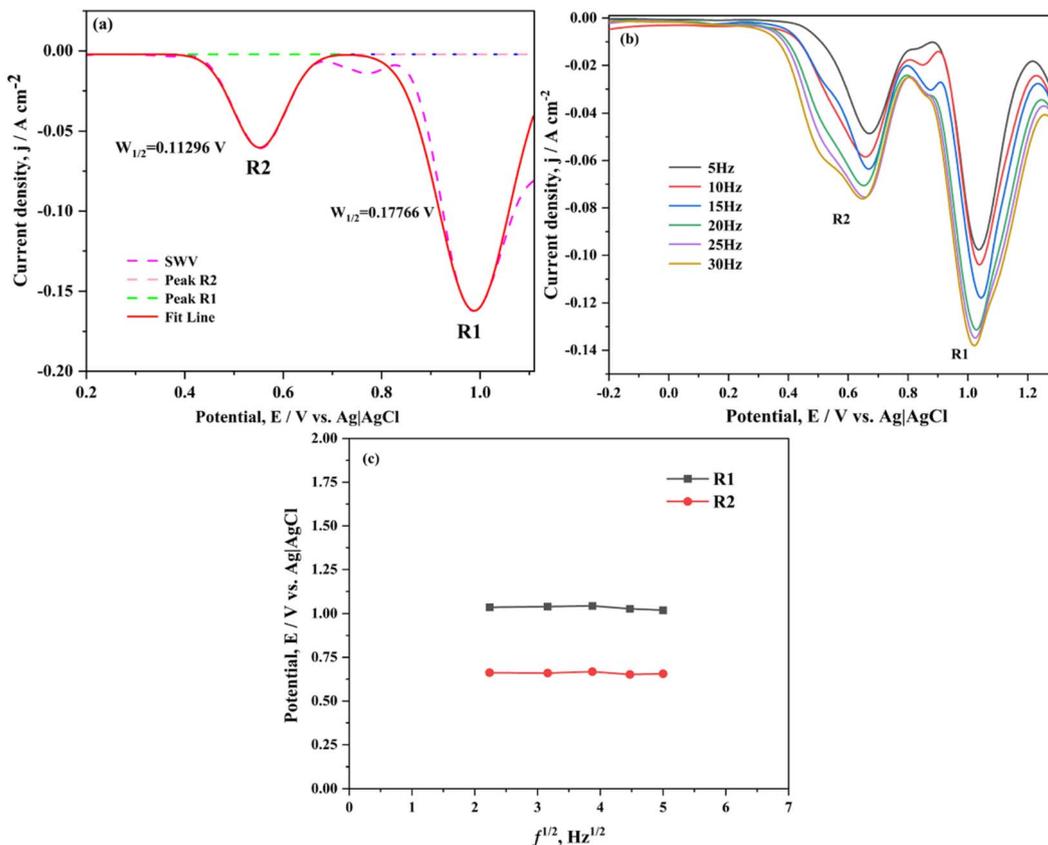
**Fig. 7** (a) Gaussian fitting of square wave voltammetry of LiCl–KCl–RuCl$_3$ at 773 K with 15 Hz. (b) Square wave voltammetry of LiCl–KCl–RuCl$_3$ ($1.13 \times 10^{-4}$ mol cm$^{-3}$) was performed on a tungsten wire electrode at varying frequencies. (c) Dependence of reduction peak potential on square root of the scan frequency for R1 and R2 for a W electrode in LiCl–KCl–RuCl$_3$ ($1.13 \times 10^{-4}$ mol cm$^{-3}$) eutectic (working electrode: W electrode, surface area: 0.32 cm$^2$; counter electrode: graphite rod ($\Phi$5.0 mm)).

electrode reaction, which corresponded to the two reduction reactions in the results of CV. SWV curves obtained at different frequencies are shown in Fig. 7(b). Fig. 7(c) shows the relationship between peak potentials R1 and R2 and the square of frequency. Within these curves, the positions of reduction

peaks R1 and R2 exhibit minimal shift with increasing scan frequency, displaying no significant displacement, while the current density shows a decreasing trend. By utilizing Origin software to fit the relationship between the square root of frequency and current density, the results are presented in
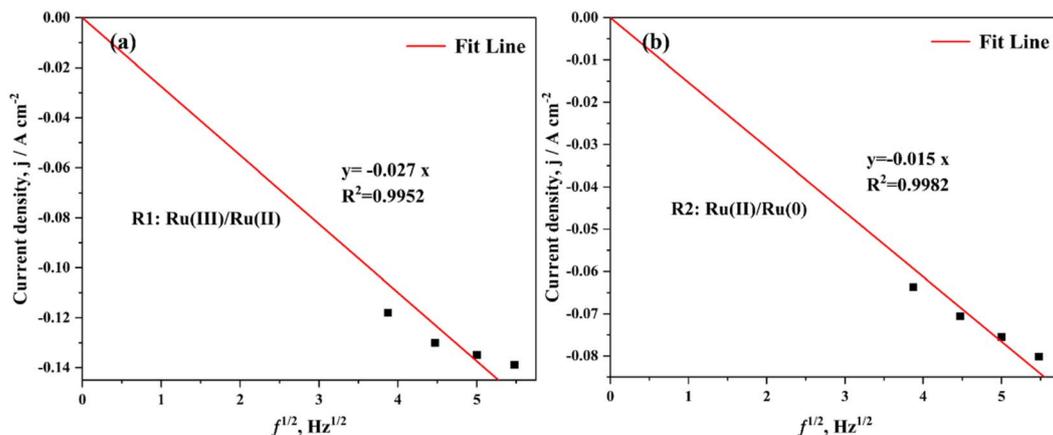


**Fig. 8** The relationship between the current density of the peak potential R1 (a) and R2 (b) of the square wave voltammetry curve of the LiCl–KCl–RuCl$_3$ ($1.13 \times 10^{-4}$ mol cm$^{-3}$) molten salt system and the square root of the scanning frequency at 773 K (working electrode: W electrode, surface area: 0.32 cm$^2$; counter electrode: graphite rod ($\Phi$5.0 mm)).
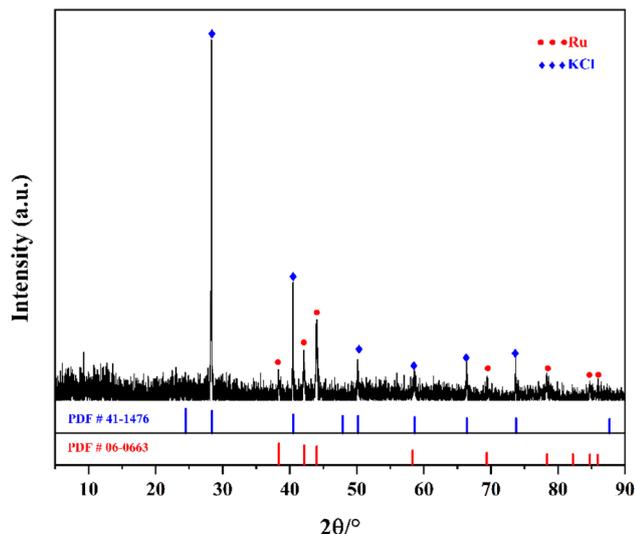
**Fig. 9** XRD pattern of the deposits in LiCl–KCl–RuCl$_3$ ($1.13 \times 10^{-4}$ mol cm$^{-3}$) system at 773 K after constant potential electrolysis for 2 h (working electrode: W electrode, surface area: 0.66 cm$^2$; counter electrode: graphite rod ($\Phi$5.0 mm)).
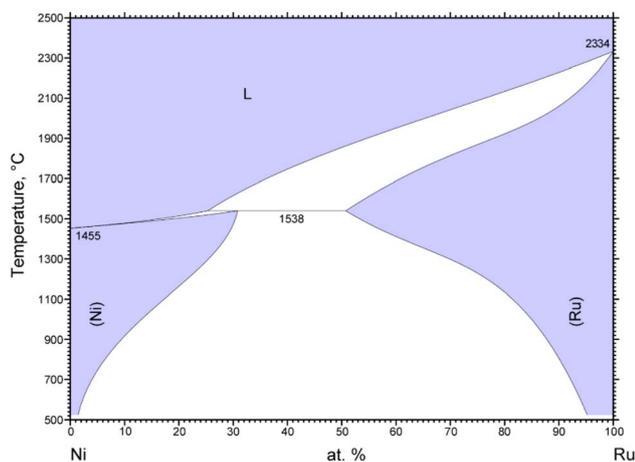


**Fig. 10** Ru–Ni binary phase diagram.[58]

Fig. 8(a)(R1) and (b)(R2). These figures reveal that the current densities of R1 and R2 exhibit a linear relationship with the square root of frequency. The above data indicate that R1 and R2 are quasi-reversible processes controlled by diffusion.

Based on the above experimental findings, the number of exchanged electrons can be calculated using the following eqn (1):[54,55]

$$W_{1/2} = 3.52 \frac{RT}{nF} \tag{1}$$

where $W_{1/2}$ denotes the half-width of the peak, $R$ (8.314 J mol$^{-1}$ K$^{-1}$) is the gas constant, $T$ represents the absolute temperature (K), $F$ is the Faraday constant (C mol$^{-1}$), and $n$ is the number of exchanged electrons in the reduction. The half-peak widths corresponding to R1 and R2 in Fig. 5(a) are 0.17766 and 0.11296, respectively. The number of exchanged electrons of R1 and R2

are calculated to be about 1 (1.31) and 2 (2.07), respectively. This proves that the observed phenomenon corresponds to the electrode reaction between Ru(III) and Ru, as shown below:

$$\text{R1: } R^{3+} + e^- = Ru^{2+}$$

$$\text{R2: } R^{2+} + 2e^- = Ru$$
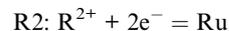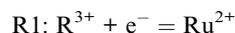
This indicates that the reduction step of Ru(III) in the LiCl–KCl system is Ru(III) → Ru(II) → Ru(0).

**3.1.3. Diffusion coefficient of Ru(III).** The above experimental results indicate that the electrochemical process of Ru(III) in the LiCl–KCl molten salt system is a diffusion-controlled quasi-reversible process. As shown in Fig. 6(a), the slope ($k$) of this line is −0.354. This slope represents the ratio of current density to the square root of the sweep velocity. Therefore, the diffusion coefficient of Ru(III) was calculated to be 1.65 × 10$^{-6}$ cm$^2$ s$^{-1}$, based on Fig. 6 and the Randles–Sevcik eqn (2)–(6):

$$\frac{I_p}{A} = 0.4463nFC\left(\frac{nF}{RT}\right)^{1/2} D^{1/2} v^{1/2} \tag{2}$$

$$\frac{I_p}{A} \bigg/ v^{1/2} = 0.4463nFC\left(\frac{nF}{RT}\right)^{1/2} D^{1/2} \tag{3}$$

$$\frac{I_p}{A} \bigg/ v^{1/2} = k \tag{4}$$

$$k = 0.4463nFC\left(\frac{nF}{RT}\right)^{1/2} D^{1/2} \tag{5}$$

$$D = k^2 \bigg/ (0.4463nFC)^2 \frac{nF}{RT} \tag{6}$$

where $I_p$ is the peak current (A), $C$ represents the bulk concentration of Ru(III) in the LiCl–KCl (mol cm$^{-3}$), $D$ denotes the diffusion coefficient of Ru(III) (cm$^2$ s$^{-1}$), $A$ refers to the surface area of the working electrode (cm$^2$), $v$ signifies the scan rate (V s$^{-1}$), and other physical quantities are the same in eqn (1). The order of magnitude of Ru's diffusion coefficient in this study is consistent with Mo and Nb in chloride molten salts, which are also noble metals.[56,57]

### 3.2. Electrolytic separation of Ru(III) ions in molten LiCl–KCl

**3.2.1. Constant-potential electrolysis experiment.** During the research process, tungsten electrodes were initially employed. Although the tungsten electrode can extract ruthenium, its ability to adhere to ruthenium during electrolysis is relatively weak. This leads to the deposited ruthenium detaching and dispersing in the molten salt, hindering the collection and analysis of the electrolytic products. A portion of the electrolytic products detached in the molten salt was collected and subjected to XRD characterization analysis. The results, presented in Fig. 9, confirmed that the electrolytic products were ruthenium. In summary, while tungsten electrodes can also achieve Ru extraction, the shedding of electrolytic products into
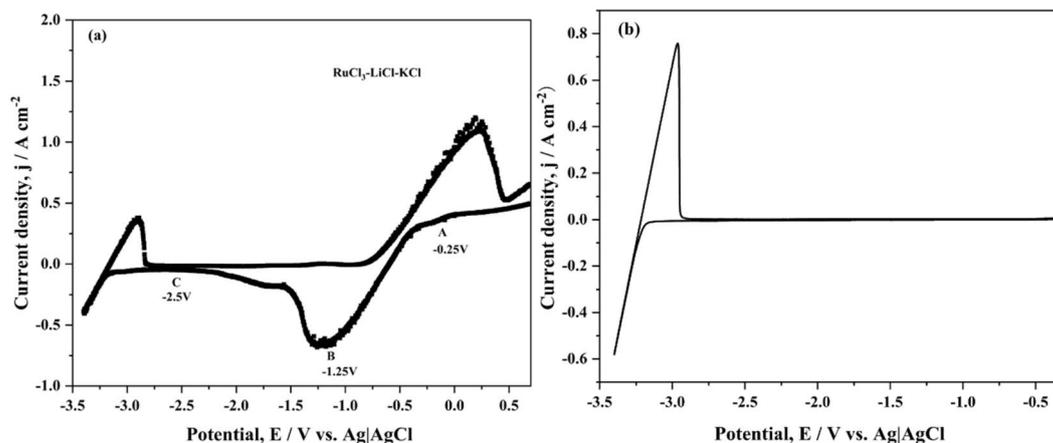
**View Article Online**

Paper                                                                    **RSC Advances**

Open Access Article. Published on 04 March 2026. Downloaded on 5/4/2026 1:37:18 AM. This article is licensed under a Creative Commons Attribution-NonCommercial 3.0 Unported Licence.

**Fig. 11** (a) Cyclic voltammetry curves of LiCl–KCl–RuCl$_3$ ($1.13 \times 10^{-4}$ mol cm$^{-3}$) systems at 773 K with the scan rate of 0.1 V s$^{-1}$. (b) The cyclic voltammetry test curve of LiCl–KCl–RuCl$_3$ ($1.13 \times 10^{-4}$ mol cm$^{-3}$) molten salt after constant potential electrolysis for 2 h at 773 K (working electrode: Ni electrode, surface area: 2.3 cm$^2$; counter electrode: graphite rod ($\Phi$5.0 mm)).



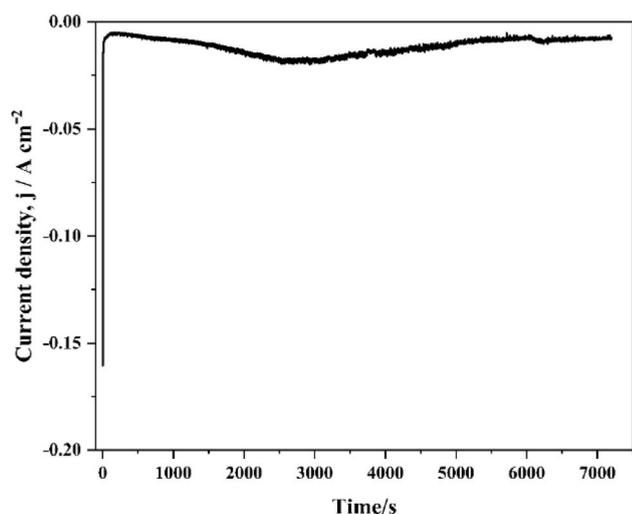**Fig. 12** Constant-potential current–time curve on nickel electrode at $-2.5$ V in LiCl–KCl–RuCl$_3$ ($1.13 \times 10^{-4}$ mol cm$^{-3}$) eutectic molten salt (working electrode: Ni electrode, surface area: 2.3 cm$^2$; counter electrode: graphite rod ($\Phi$5.0 mm); temperature: 773 K).

the molten salt during the process hinders the collection and analysis of these products. Therefore, nickel electrodes were selected for subsequent research.

As shown in Fig. 10, a nickel plate is an inert electrode because ruthenium does not form an alloy with nickel (Ni).[58] CV curve results for measuring ruthenium ions using a nickel plate as the working electrode are shown in Fig. 11(a). As can be seen from the diagram, the Ru current on the electrode begins to appear at A ($-0.25$ V), with the maximum electrolytic current of $-0.73$ A cm$^{-2}$ peaking at B ($-1.25$ V). Consequently, it can be inferred that the reduction potential of Ru on the Ni electrode is $-1.25$ V. Therefore, the potential selection for electrolyzing ruthenium should be more negative than $-1.25$ V; that is, the potential range should be controlled between $-1.25$ V and the potential of Li$^+$ reduction. Based on this, the system RuCl$_3$–LiCl–KCl was electrolyzed at a constant potential of C ($-2.5$ V) at 773 K using a nickel sheet in this experiment. Theoretically, at this potential, ruthenium can be effectively electrolyzed. After electrolysis of 2 h, the electrolysis curve shown in Fig. 12 was obtained, and the deposits on the electrode surface are shown



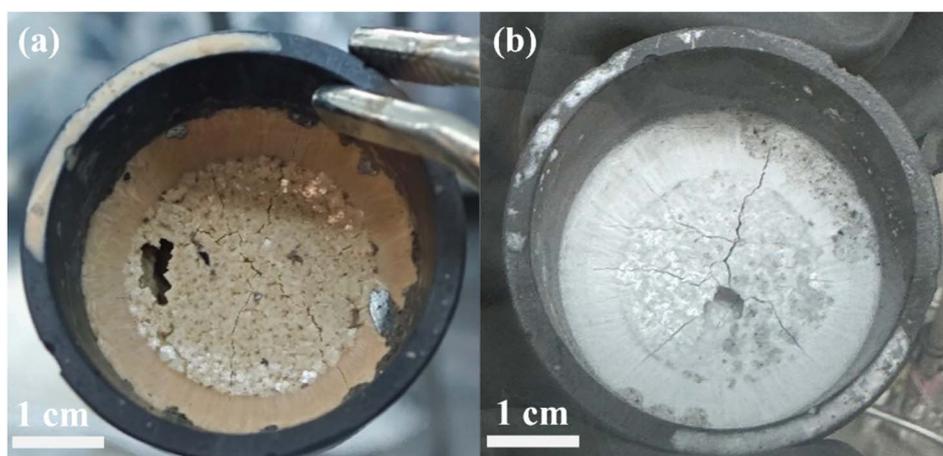**Fig. 13** Color change diagram of salt blocks before (a) and after (b) constant potential electrolysis for 2 h.

© 2026 The Author(s). Published by the Royal Society of Chemistry                    RSC Adv., 2026, **16**, 12360–12373 | **12367**
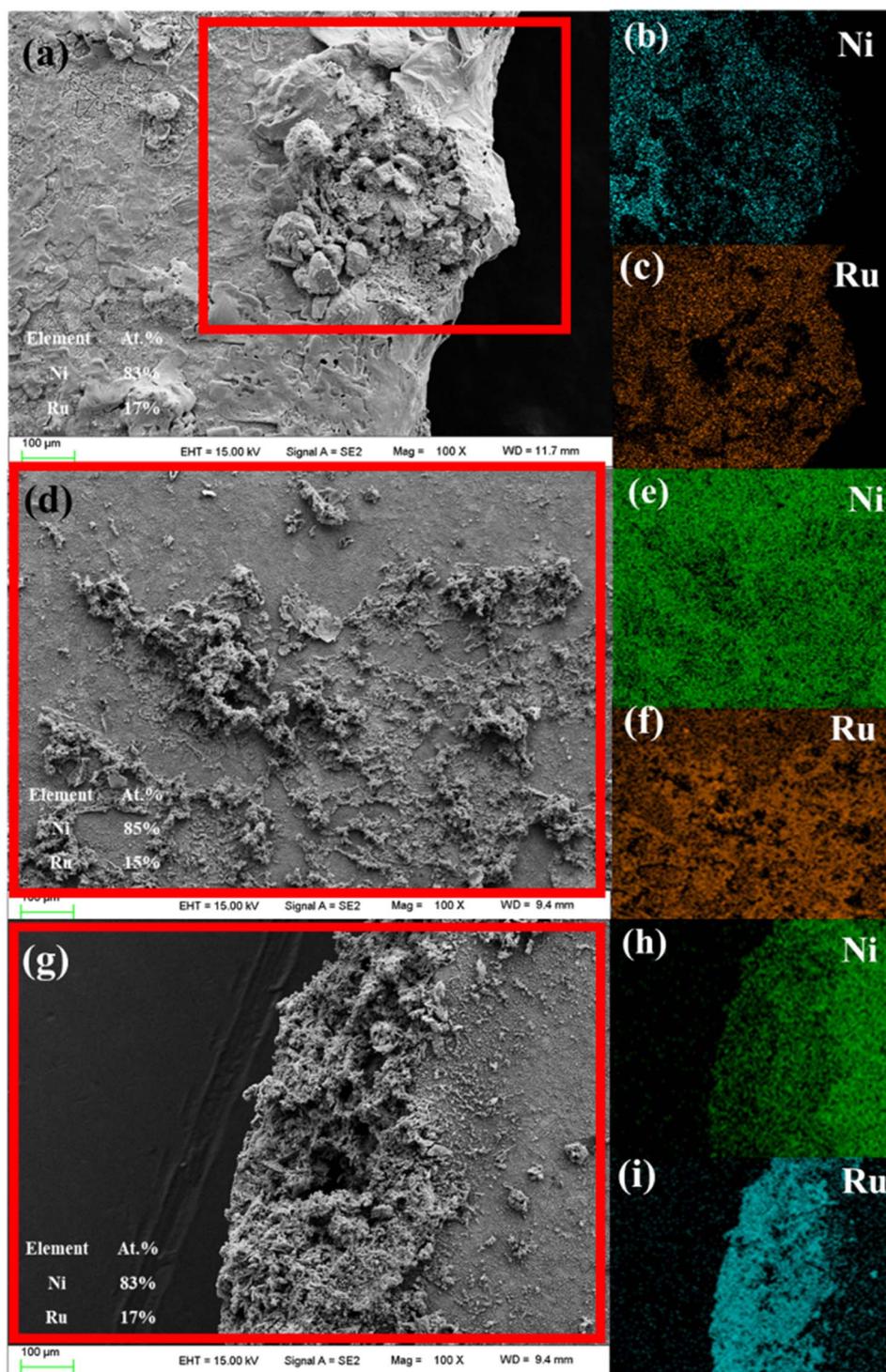
**Fig. 14** SEM patterns (a, d and g) and EDS charts (b, c, e, f, h and i) of surface scan about the deposits obtained on the nickel electrode after constant potential electrolysis at − 2.5 V and 773 K for 2 h.

in Fig. 16(a). Deposits were obtained on the nickel electrode and the surface was covered with a small amount of residual molten salt medium. The CV curve test of the molten salt after electrolysis showed that there were no other redox peaks except for a pair of redox peaks of $Li^+$ in Fig. 11(b). In addition, as shown in Fig. 13, $RuCl_3$–LiCl–KCl molten salt exhibits an orange color

(Fig. 13(a)) before electrolysis. Following electrolysis, the color of $RuCl_3$–LiCl–KCl molten salt changes to white (Fig. 13(b)), which is similar to LiCl–KCl molten salt.

**3.2.2. Characterization of electrolysis products.** The sample can be washed with water. During washing, metallic ruthenium is insoluble in water,[59,60] while the LiCl–KCl salt can
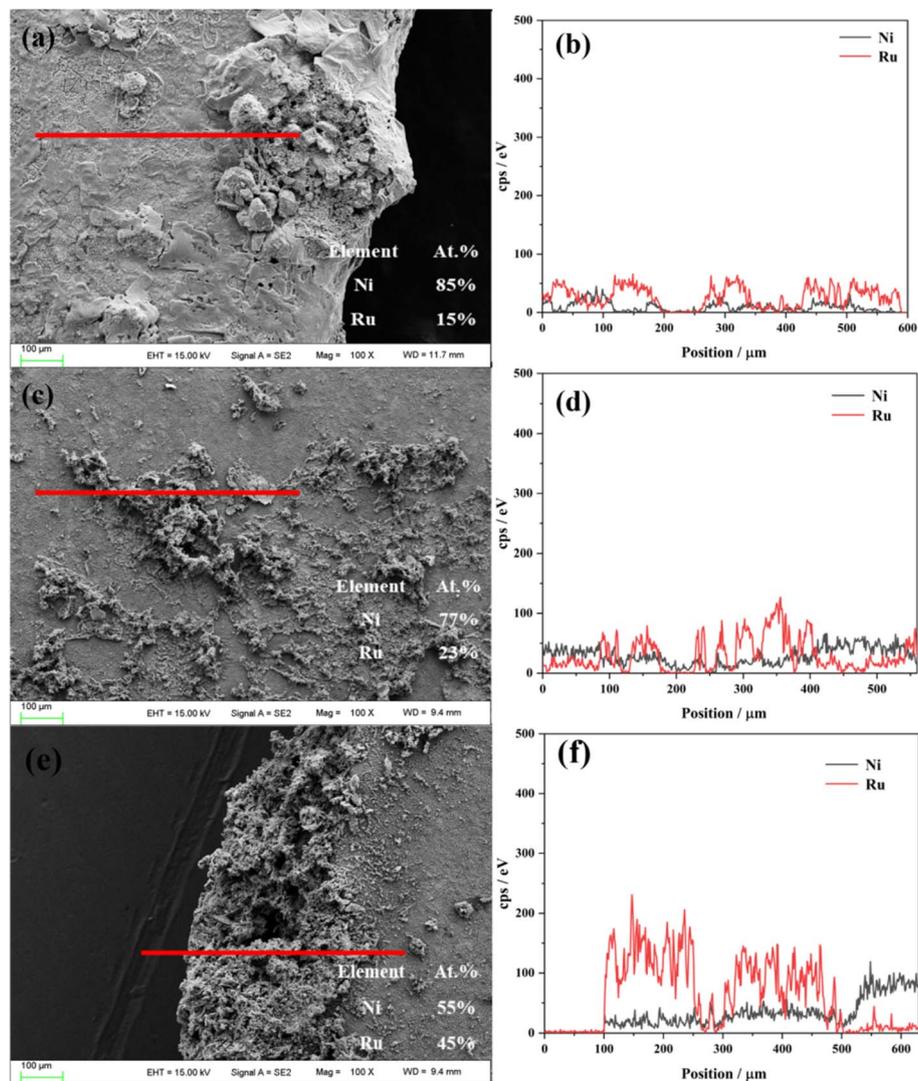
Fig. 15 SEM patterns (a, c and e) and EDS charts (b, d and f) of line scan about the deposits obtained on the nickel electrode after constant potential electrolysis at − 2.5 V and 773 K for 2 h.
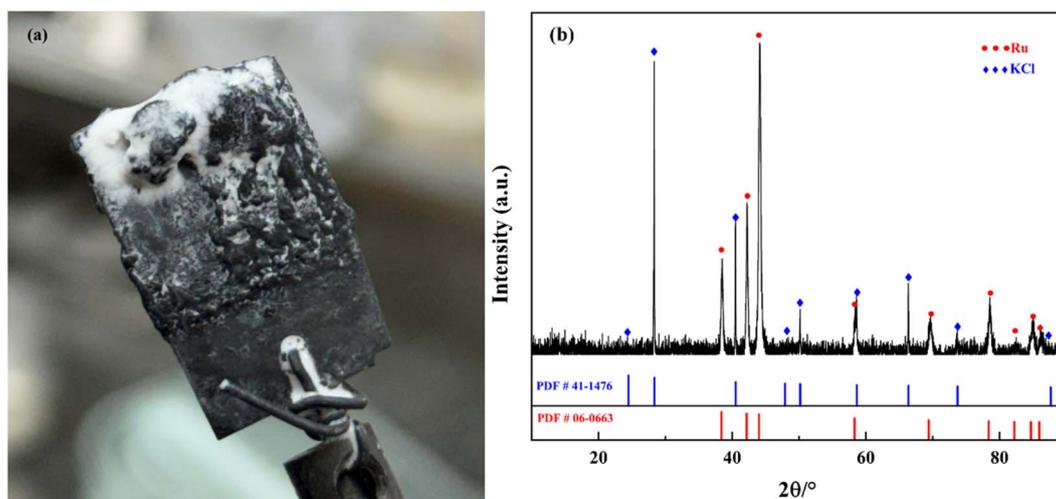


Fig. 16 (a) Electrolysis products acquired from nickel electrode in LiCl–KCl–RuCl$_3$ ($1.13 \times 10^{-4}$ mol cm$^{-3}$) eutectic molten salt mixed salts after constant potential electrolysis for 2 h at 773 K. (b) XRD pattern of the deposits in the LiCl–KCl–RuCl$_3$ ($1.13 \times 10^{-4}$ mol cm$^{-3}$) system at 773 K after constant potential electrolysis for 2 h (working electrode: Ni electrode, surface area: 2.3 cm$^2$; counter electrode: graphite rod ($\Phi$5.0 mm)).

**Fig. 17** XRD patterns of the electrolytic products before (a) and after (b) washing in LiCl–KCl–RuCl$_3$ ($1.13 \times 10^{-4}$ mol cm$^{-3}$) system at 773 K after constant potential electrolysis for 2 h (working electrode: Ni electrode, surface area: 2.3 cm$^2$; counter electrode: graphite rod ($\Phi$5.0 mm)).

be washed away. Following electrolysis, the products were treated with ultrasonic cleaning and vacuum drying and subsequently analyzed by XRD and SEM-EDS. Fig. 14 displays the SEM image of diff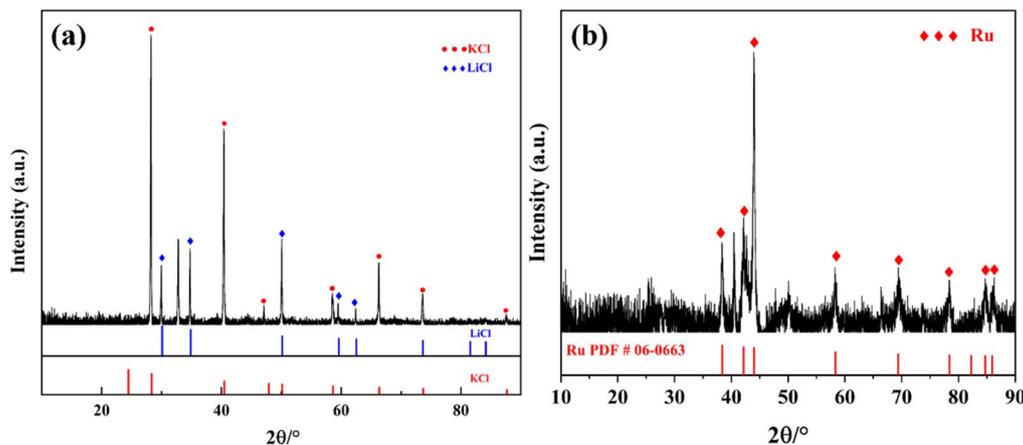erent regions of the electrolytic products obtained by constant potential electrolysis at −2.5 V. EDS of the surface scan in Fig. 14(b, c, e, f, h and i) and the line scan in Fig. 15(b, d and f) were swept to the Ru element. The XRD characterization diagram is provided in Fig. 16(b), which indicates that the primary composition of the electrolytic product is Ru metal. Fig. 17 shows the XRD patterns of the electrolytic products before (Fig. 17(a)) and after (Fig. 17(b)) washing. The XRD pattern clearly demonstrates the high purity of Ru after washing. The XRD characterization shows that the Ru detected by EDS corresponds to Ru metal obtained through electrolysis, not RuCl$_3$ added to the system. The results of electrolytic separation characterization confirm the precision of the Ru(III) electrochemical behavior analysis and further verify that the hypothesis of the reduction mechanism of Ru(III) was reasonable.

**3.2.3. Electrolysis efficiency and feasibility analysis.** After the completion of electrolysis, a small amount of sample was taken from the molten salt, and the Ru(III) concentration was measured using ICP-OES. The extraction efficiency ($\xi$) was estimated using the following formula and Table 2:

$$\xi = \frac{c_i - c_f}{c_i} \qquad (7)$$

where $c_i$ and $c_f$ represent the initial and final concentrations of Ru(III) in LiCl–KCl molten salt, respectively.

The extraction efficiency ($\xi$) of ruthenium ions after 2 h electrolysis at −2.5 V is 88.92%. Subsequently, the charges at different

**Table 2** Concentration of Ru before and after electrolysis and corresponding peak current values in LiCl–KCl molten salt

| | Concentration of Ru/mol cm$^{-3}$ | Peak current/A cm$^{-2}$ |
|---|---|---|
| Before electrolysis | $1.13 \times 10^{-4}$ | −0.73 |
| After electrolysis | $1.22 \times 10^{-5}$ | $-4.24 \times 10^{-4}$ |

electrolysis potentials were integrated, and the corresponding current efficiency was calculated using eqn (8) and Fig. 8.

$$\eta = \frac{\dfrac{m_{\text{cathode}}}{M_V} nF}{3600 I t} \times 100\% \qquad (8)$$

where $\eta$ is cathode current efficiency of Ru deposition; $m_{\text{cathode}}$ is weight of metallic ruthenium on cathode, g; $M_V$ is molecular mass of metallic ruthenium, 101.07 g mol$^{-1}$; $I$ is current, A; $t$ is time, h. The current efficiency was 58.93% for constant-potential electrolysis for 2 h.

All experimental results illustrate that the electrolytic separation of Ru can be achieved by using a nickel sheet for constant potential electrolysis at −2.5 V for 2 hours. This further confirms the feasibility of electrolytic separation of Ru in LiCl–KCl molten salt.

## 4 Conclusion

The electrochemical behavior of Ru(III) in LiCl–KCl molten salt at 773 K was investigated using CV and SWV. The results indicate that the reduction of Ru(III) in LiCl–KCl molten salt involves a two-step process: Ru(III) → Ru(II) → Ru(0). It also demonstrates that the electrochemical process of Ru(III) in the LiCl–KCl molten salt system is a diffusion-controlled quasi-reversible process. The diffusion coefficients of Ru(III) were analyzed and calculated, and the values of $1.65 \times 10^{-6}$ cm$^2$ s$^{-1}$ were obtained.

Subsequently, the constant potential electrolysis method was used to electrolyze ruthenium, and the electrolysis products were analyzed by XRD and SEM-EDS. The results showed that the electrolysis products were ruthenium metal. Moreover, the concentration of Ru by ICP-OES shows a marked decrease both before and after electrolysis. Furthermore, test results obtained using ICP-OES estimated the extraction efficiency of Ru throughout the entire electrolysis process to be 88.92%. Finally, the current efficiency in the whole electrolysis process was calculated to be 58.93%. All research results demonstrate that the electrochemical separation of ruthenium in LiCl–KCl molten salt is feasible.

This work revealed the electrochemical reduction mechanism and electrolytic deposition process of ruthenium ions in LiCl–KCl molten salt, which provides a theoretical basis and data support for continuing to explore the reduction mechanism of ruthenium ions in other molten salts. In addition, this work provides a feasible route for electrolysis and preparation of metallic Ru in a new system. In subsequent work, we will continue to study the reduction mechanism and electrolytic deposition process of ruthenium in fluoride salts. At the same time, we will promote process optimization to improve current efficiency. Subsequently, further purification processes will be designed to refine the crude product obtained by electrolysis, and finally a high-purity ruthenium product will be obtained.

In future work, the separation efficiency of this technology will be further validated under more realistic application conditions, with a particular focus on assessing the feasibility of isolating ruthenium from complex mixed fission product systems. Finally, a techno-economic evaluation will be performed on the entire process flow, including ruthenium separation and purification. This will ultimately establish a complete extraction and separation process for obtaining high-purity Ru products, integrating both technical feasibility and economic rationality into the process flow.

## Author contributions

Lei Wang: conceptualization, methodology, investigation, formal analysis, writing—original draft. Hao Peng: conceptualization, formal analysis, funding acquisition. Yahui Wang: investigation. Lifang Tian: visualization, investigation. Hailang Li: methodology, formal analysis. Qiang Dou: writing—review and editing, funding acquisition, methodology, formal analysis. Haiying Fu: writing—review and editing, conceptualization, methodology, formal analysis. All authors reviewed the manuscript.

## Conflicts of interest

The authors declare no conflicts of interest.

## Abbreviations

| $\varphi$ | Diameter, mm |
|---|---|
| $\varphi$ | Specifications, mm |
| $W_{1/2}$ | Half-peak widths, V |
| $R$ | Gas constant J mol$^{-1}$ K$^{-1}$ |
| $T$ | Absolute temperature, K |
| $n$ | Number of exchanged electrons, – |
| $F$ | Faraday constant, C mol$^{-1}$ |
| $I_p$ | Peak current, A |
| $c$ | Bulk concentration, mol cm$^{-3}$ |
| $D$ | Diffusion coefficient, cm$^2$ s$^{-1}$ |
| $A$ | Surface area, cm$^2$ |
| $v$ | Scan rate V s$^{-1}$ |
| $c_i$ | Initial concentrations, mol cm$^{-3}$ |
| $c_f$ | Final concentrations, mol cm$^{-3}$ |
| $\xi$ | Extraction efficiencies, - |
| $\eta$ | Cathode current efficiency, - |
| $M_v$ | Molecular mass, g mol$^{-1}$ |
| $I$ | Current, A |
| $t$ | Time, s |
| CV | Cyclic voltammetry |
| SWV | Square wave voltammetry |
| XRD | X-ray diffraction |
| SEM | Scanning electron microscopy |
| EDS | Energy-dispersive spectroscopy |
| ICP-OES | Inductively Coupled Plasma-Optical Emission Spectrometer |

## Data availability

Data will be made available on request. All the data discussed in this study are represented in the figures and shown in this work.

## References

1 W. R. Grimes, Molten-salt reactor chemistry, *Nucl. Appl. Technol.*, 1970, **8**(2), 137–155.

2 M. T. Robinson, Jr W. A. Brooksbank, S. A. Reynolds, *et al.*, The behavior of fission products in molten fluoride reactor fuels, *Nucl. Sci. Eng.*, 1958, **4**(3), 288–296.

3 E. L. Compere, S. S. Kirslis and E. G. Bohlmann, *et al.*, *Fission Product Behavior in the Molten Salt Reactor experiment[R]*, Oak Ridge National Lab. (ORNL), Oak Ridge, TN (United States), 1975.

4 R. J. Kedl, *Migration of a Class of Fission Products (Noble Metals) in the Molten-Salt Reactor Experiment[R]*, Oak Ridge National Lab. (ORNL), Oak Ridge, TN (United States), 1972.

5 M. W. Rosenthal, R. B. Briggs and P. R. Kasten, *Molten-Salt Reactor Program Semiannual Progress Report*, ORNL-4548, 1970, pp. 111–118.

6 C. Degueldre, J. Findlay, D. Cheneler, *et al.*, Short life fission products extracted from molten salt reactor fuel for radiopharmaceutical applications, *Appl. Radiat. Isot.*, 2024, **205**, 111146.

7 M. Thery, A. C. Bonraisin, C. Alliot, *et al.*, Chromatographic-based $^{103}$Ru/$^{103m}$Rh generator for Auger Therapy, *J. Chromatogr. A*, 2025, 466149.

8 G. Skarnemark, A. Ödegaard-Jensen, J. Nilsson, *et al.*, Production of $^{103m}$Rh for cancer therapy, *J. Radioanal. Nucl. Chem.*, 2009, **280**(2), 371–373.

9 B. Happl, T. Balber, P. Heffeter, *et al.*, Synthesis and preclinical evaluation of BOLD-100 radiolabeled with

ruthenium-97 and ruthenium-103, *Dalton Trans.*, 2024, **53**(13), 6031–6040.

10 R. Herken and M. Wenzel, Autoradiographical investigations on the affinity of acetyl-($^{103}$Ru)-ruthenocene for the adrenal glands of mice, *Eur. J. Nucl. Med.*, 1985, **10**(1), 56–59.

11 N. M. Rezayee, C. A. Huff and M. S. Sanford, Tandem amine and ruthenium-catalyzed hydrogenation of $CO_2$ to methanol, *J. Am. Chem. Soc.*, 2015, **137**(3), 1028–1031.

12 Z. Cheng, Z. Zhao, J. Geng, *et al.*, The distribution and behavior of noble metal fission products ($^{99}$Mo, $^{103}$Ru, $^{105}$Rh and $^{132}$Te) in molten 2LiF-BeF$_2$ mixtures, *J. Nucl. Mater.*, 2022, **566**, 153807.

13 G. D. DelCul, L. D. Trowbridge and J. P. Renier, *et al. Analysis of the Reuse of Uranium Recovered from the Reprocessing of Commercial LWR Spent fuel[R]*, Oak Ridge National Lab. (ORNL), Oak Ridge, TN (United States), 2009.

14 M. W. Rosenthal, *The Development Status of Molten-Salt Breeder Reactors*. ORNL-4812, 1972.

15 J. Lacquement, H. Boussier, A. Laplace, *et al.*, Potentialities of fluoride-based salts for specific nuclear reprocessing: overview of the R&D program at CEA, *J. Fluorine Chem.*, 2009, **130**(1), 18–21.

16 G. L. Fredrickson, G. Cao, P. K. Tripathy, *et al.*, Electrochemical measurements in molten salt systems: a guide and perspective, *J. Electrochem. Soc.*, 2019, **166**(13), D645.

17 T. Williams, R. Shum and D. Rappleye, Concentration measurements in molten chloride salts using electrochemical methods, *J. Electrochem. Soc.*, 2021, **168**(12), 123510.

18 M. M. Tylka, J. L. Willit, J. Prakash, *et al.*, Application of voltammetry for quantitative analysis of actinides in molten salts, *J. Electrochem. Soc.*, 2015, **162**(12), H852.

19 G. Mamantov and D. L. Manning, Voltammetry and Related Studies of Uranium in Molten Lithium Fluoride-Beryllium Fluoride-Zirconium Fluoride, *Anal. Chem.*, 1966, **38**(11), 1494–1498.

20 L. Yichuan, L. Yalan, J. Shilin, *et al.*, Recent progress on chemical species of uranium in molten chlorides, *Acta Chim. Sin.*, 2021, **79**(12), 1425.

21 S. Geran, P. Chamelot, J. Serp, *et al.*, Electrochemistry of uranium in molten LiCl-LiF, *Electrochim. Acta*, 2020, **355**, 136784.

22 C. Hamel, P. Chamelot, A. Laplace, *et al.*, Reduction process of uranium (IV) and uranium (III) in molten fluorides, *Electrochim. Acta*, 2007, **52**(12), 3995–4003.

23 F. Jiang, W. Huang, H. Zheng, *et al.*, Electrochemical behavior and electrowinning of uranium (IV) from FLiNaK molten salt, *J. Radioanal. Nucl. Chem.*, 2017, **311**(3), 1891–1897.

24 M. Straka, M. Korenko and F. Lisý, Electrochemistry of uranium in LiF–BeF$_2$ melt, *J. Radioanal. Nucl. Chem.*, 2010, **284**(1), 245–252.

25 X. Wang, W. Huang, Y. Gong, *et al.*, Electrochemical behavior of Th (IV) and its electrodeposition from ThF$_4$-LiCl-KCl melt, *Electrochim. Acta*, 2016, **196**, 286–293.

26 K. Liu, L. Y. Yuan, Y. L. Liu, *et al.*, Electrochemical reactions of the Th$^{4+}$/Th couple on the tungsten, aluminum and bismuth electrodes in chloride molten salt, *Electrochim. Acta*, 2014, **130**, 650–659.

27 X. Wang, H. Zheng, Q. Xu, *et al.*, Electrochemical behaviors and electrolytic separation of Th (IV) and Ce (III) in ThF$_4$-CeF$_3$-LiCl-KCl quaternary melt, *Sep. Purif. Technol.*, 2019, **210**, 236–241.

28 M. R. Bermejo, J. Gómez, J. Medina, *et al.*, The electrochemistry of gadolinium in the eutectic LiCl–KCl on W and Al electrodes, *J. Electroanal. Chem.*, 2006, **588**(2), 253–266.

29 Y. D. Yan, Y. L. Xu, M. L. Zhang, *et al.*, Electrochemical extraction of neodymium by co-reduction with aluminum in LiCl–KCl molten salt, *J. Nucl. Mater.*, 2013, **433**(1–3), 152–159.

30 X. Li, Y. D. Yan, M. L. Zhang, *et al.*, Extraction of ytterbium *via* co-reduction of Al (III) and Yb (III) from LiCl-KCl melt on W electrode, *J. Radioanal. Nucl. Chem.*, 2014, **299**(1), 657–664.

31 Y. L. Liu, L. Y. Yuan, G. A. Ye, *et al.*, Electrochemical extraction of samarium from LiCl–KCl melt by forming Sm–Zn alloys, *Electrochim. Acta*, 2014, **120**, 369–378.

32 Y. Castrillejo, P. Fernández, M. R. Bermejo, *et al.*, Electrochemistry of thulium on inert electrodes and electrochemical formation of a Tm–Al alloy from molten chlorides, *Electrochim. Acta*, 2009, **54**(26), 6212–6222.

33 Y. Castrillejo, M. R. Bermejo, E. Barrado, *et al.*, Electrochemical behaviour of erbium in the eutectic LiCl–KCl at W and Al electrodes, *Electrochim. Acta*, 2006, **51**(10), 1941–1951.

34 R. Chesser, S. Guo and J. Zhang, Electrochemical behavior of dysprosium and lanthanum in molten LiF-NaF-KF (FLiNaK) salt, *Ann. Nucl. Energy*, 2018, **120**, 246–252.

35 G. Lacarbonara, S. Chini, S. Ratso, *et al.*, A MnOx–graphitic carbon composite from $CO_2$ for sustainable Li-ion battery anodes, *Mater. Adv.*, 2022, **3**(18), 7087–7097.

36 E. Najafli, S. Ratso, Y. P. Ivanov, *et al.*, Sustainable $CO_2$-derived nanoscale carbon support to a platinum catalyst for oxygen reduction reaction, *ACS Appl. Nano Mater.*, 2023, **6**(7), 5772–5780.

37 J. Ge, D. Zhang, Y. Qin, *et al.*, Dual-metallic single Ru and Ni atoms decoration of MoS$_2$ for high-efficiency hydrogen production, *Appl. Catal., B*, 2021, **298**, 120557.

38 Y. Kobayashi, H. Yamatera and H. Okuno, The electrodeposition of ruthenium from a ruthenium (III) and ruthenium (IV) solution and a fission products solution, *Bull. Chem. Soc. Jpn.*, 1965, **38**(11), 1911–1915.

39 P. Swain, C. Mallika, C. Jagadeeswara Rao, *et al.*, Electrochemical studies on the reduction behaviour of ruthenium nitrosyl ions in nitric acid medium, *J. Appl. Electrochem.*, 2015, **45**(2), 209–216.

40 R. Zou, Y. Wang, M. Hu, *et al.*, Analysis of ruthenium electrodeposition in the nitric acid medium, *J. Phys. Chem. C*, 2022, **126**(9), 4329–4337.

41 A. A. Osipenko and V. A. Volkovich, Study of ruthenium behavior in alkali chloride melts using electronic absorption spectroscopy[C], *AIP Conf. Proc.*, 2019, 020045.

42 A. A. Osipenko , V. A. Volkovich. Ruthenium behaviour in alkali chloride melts[C]//PHYSICS, TECHNOLOGIES AND INNOVATION (PTI-2018): *Proceedings of the V International Young Researchers' Conference.*2018.

43 I. V. May, A. Volkovich, *et al. An EXAFS Spectroscopy Study of Speciation of Uranium and Some Fission Product Elements in Chloride Melts*, 2004.

44 G. K. Sireli, An investigation of ruthenium coating from LiCl–KCl eutectic melt, *Appl. Surf. Sci.*, 2014, **317**(oct.30), 294–301.

45 V. Periasamy, P. N. N. Elumalai, S. Talebi, *et al.*, Novel same-metal three electrode system for cyclic voltammetry studies, *RSC Adv.*, 2023, **13**(9), 9.

46 W. Qi, J. Xu, Y. Yuan, *et al.*, Molten salt electrophoretic deposition of $TiB_2$ coatings on C/C composites in a three-electrode system: preparation and high-temperature oxidation resistance, *Ceram. Int.*, 2025, **51**, 57392–57402.

47 J. Zhang, Electrochemistry of actinides and fission products in molten salts—Data review, *J. Nucl. Mater.*, 2014, **447**(1–3), 271–284.

48 J. Zhang, B. Hu, H. Qiao, *et al.*, Thermodynamic Modeling of the Re–Ru, Ru–W and Re–Ru–W Systems, *J. Phase Equilib. Diffus.*, 2021, **42**(4), 489–498.

49 Q. Liu, Y. Chen, Z. Dong, *et al.*, Electrochemical separation of fission element neodymium using plumbum electrode from molten LiCl–KCl based on spent fuel reprocessing, *Prog. Nucl. Energy*, 2023, **163**, 104819.

50 H. Peng, M. Shen, Y. Zuo, *et al.*, Electrochemical technique for detecting the formation of uranium-containing precipitates in molten fluorides, *Electrochim. Acta*, 2016, **222**, 1528–1537.

51 J. Wang, T. Nakazato, K. Sakanishi, *et al.*, Microwave digestion with $HNO_3/H_2O_2$ mixture at high temperatures for determination of trace elements in coal by ICP-OES and ICP-MS, *Anal. Chim. Acta*, 2004, **514**(1), 115–124.

52 O. Shirai, T. Iwai, Y. Suzuki, *et al.*, Electrochemical behavior of actinide ions in LiCl–KCl eutectic melts, *J. Alloys Compd.*, 1998, **271**, 685–688.

53 F. Jiang, N. Ji, W. Huang, *et al.*, The electrochemical behavior of neodymium (III) in FLiNaK molten salt on Pt cathode, *J. Electrochem. Soc.*, 2022, **169**(10), 102505.

54 X. Xi, J. Wang, J. Zhang, *et al.*, Electrochemical behavior and separation of Ce (III) in LiCl-KCl molten salt, *Sep. Purif. Technol.*, 2024, **334**, 125931.

55 H. Lv, L. Zhang, X. Xi, *et al.*, Electrochemical dissolution, reduction, and nucleation mechanisms of molybdenum in NaCl-KCl molten salt systems, *J. Mater. Sci. Technol.*, 2025, **238**, 45–54.

56 H. Zhang, Z. Lv, S. Li, *et al.*, Electrochemical behavior of molybdenum ions and their coordination structures in NaCl-KCl melt containing fluoride ions, *J. Mol. Liq.*, 2025, **426**, 127375.

57 Z. Zhao, D. Jiang, Y. Chen, *et al.*, $K_3NbF_7$'s electrochemical characteristics in the NaCl–KCl molten salt system at the Mo electrode, *Electrochem. Commun.*, 2025, 107943.

58 P. Villars, PAULING FILE, in *Inorganic Solid Phases (Online Database)*, Springer Materials, Heidelberg, 2016.

59 P. Swain, C. Mallika and R. Srinivasan, Separation and recovery of ruthenium: a review, *J. Radioanal. Nucl. Chem.*, 2013, **298**(2), 781–796.

60 A. K. Sahu, D. K. Dash, K. Mishra, *et al.*, Properties and applications of ruthenium[M]//Noble and precious metals-properties, *Nanoscale Effects and Applications*. IntechOpen, 2018.